Ultrasonic wave propagation in stereo-lithographical bone replicas

Haydar Aygün[a)]
Medical Physics, Post-Graduate Medical Institute, The University of Hull, Cottingham Road, Hull HU6 7RX, United Kingdom

Keith Attenborough
Department of Design, Development, Environment and Materials, The Open University, Milton Keynes MK7 6AA, United Kingdom

Walter Lauriks
Laboratorium voor Akoestiek en Thermische Fysica, Katholieke Universiteit Leuven, Celestijnenlaan 200 D, B-3001 Heverlee, Belgium

Christian M. Langton
Department of Medical Physics, Queensland University of Technology, 2 George Street, Brisbane QLD 4001, Australia

(Received 12 February 2010; revised 22 March 2010; accepted 26 March 2010)

Predictions of a modified anisotropic Biot–Allard theory are compared with measurements of pulses centered on 100 kHz and 1 MHz transmitted through water-saturated stereo-lithographical bone replicas. The replicas are 13 times larger than the original bone samples. Despite the expected effects of scattering, which is neglected in the theory, at 100 kHz the predicted and measured transmitted waveforms are similar. However, the magnitude of the leading negative edge of the waveform is overpredicted, and the trailing parts of the waveforms are not predicted well. At 1 MHz, although there are differences in amplitudes, the theory predicts that the transmitted waveform is almost a scaled version of that incident in conformity with the data.
 [DOI: 10.1121/1.3397581]

PACS number(s): 43.80.Cs, 43.80.Qf, 43.80.Vj [CCC] Pages: 3781–3789

I. INTRODUCTION

Understanding the propagation of acoustic waves through cancellous bone is an important pre-requisite to improving the prediction of fracture risk by ultrasound. Bone essentially has two types of structure, both having the same mineralized collagen composition. Cortical bone may generally be considered to be solid; cancellous bone consists of a complex open-celled porous network of rod- and plate-shaped elements termed trabeculae. The porosity of human cancellous bone ranges between 70% and 95%, the remaining volume being perfused with bone marrow. In the adult human vertebral body for example, both horizontal and vertical trabeculae range from 50–120 μm in thickness, and spaced at intervals of between 1200–5000 and 700–2000 μm, respectively (Thomsen *et al.*, 2002).

Two mechanisms give rise to the structure of bone, modeling and remodeling. "Modeling" is the process primarily responsible for maintaining bones in their correct shape as they grow and respond to their biomechanical environment; it also controls the cortical thickness and marrow cavity diameter of bones as they age. "Remodeling" is mainly concerned with the continual replacing of old cancellous bone and occurs at discrete foci on the surface of the trabeculae (Frost *et al.*, 2001). During remodeling, osteoclast cells create a resorption cavity that is subsequently filled with new collagen by osteoblast cells. In osteoporosis, there is a symptomatic negative imbalance in remodeling, thereby creating a bone loss, particularly at sites of predominantly cancellous bone such as the spine, hip, wrist, and heel; this ultimately leads to skeletal fragility and increased risk of fracture (Rosen, 2004).

The conventional method of assessing osteoporosis in the clinical environment is bone mineral density (BMD, g cm^{-2}), an areal parameter describing the bone mineral content within a projected area. BMD is generally measured at sites most at risk of osteoporotic fracture, the spine, hip, and wrist. BMD is generally measured using the technique of dual energy X-ray absorptiometry (DXA) (Njeh and Shepherd, 2004). True volumetric bone density may be derived using quantitative computed tomography (QCT), utilizing a conventional CT scanner, a calibration phantom being scanned with the subject to convert Hounsfield numbers into g cm^{-3} (Lang, 2004). QCT is increasingly being used, particularly at the lumbar spine although there is a higher radiation dose compared to DXA. Although generally utilized as a research tool for the measurement of excised tissue samples, microCT provides a typical spatial resolution of 0.01 mm and hence replicates the true trabecular structure, compared to resolutions of approximately 1 mm for DXA, and slightly better than 1 mm for QCT. A technique that is gaining in-

[a)]Author to whom correspondence should be addressed. Electronic mail: h.aygun@hull.ac.uk

creasing interest is magnetic resonance (MR) imaging which essentially measures the water content of tissues. Bone does not therefore give an MR signal, although its presence may be inferred from a "negative" image (Pothuaud and Majumdar, 2004).

Quantitative ultrasound (QUS) generally involves measurements of the transmission of ultrasonic signals, either along a cortical bone surface or through a bone such as the heel and phalanx (Njeh *et al.*, 1997). There are two fundamental measurement parameters, velocity (ms^{-1}) and attenuation (dB). Velocity is obtained by dividing the propagation distance by the corresponding transit time, with through-transmission measurements recorded at the calcaneus (heel) and phalanx, and surface-transmission recorded primarily at the tibia. This technique is only correct in the absence of dispersion. If dispersion is present (which is the case in poroelastic media), this technique gives wrong results (Haiat *et al.*, 2006). Attenuation is generally expressed as broadband ultrasound attenuation (BUA, dB MHz^{-1}) at the calcaneus, describing the linear increase in attenuation with frequency between 200 and 600 kHz. It has been clinically demonstrated that velocity provides higher precision, expressed as CV%, whereas BUA exhibits higher dynamic range. It is generally accepted that of the QUS options, BUA measurement at the calcaneus provides the most accurate indication of osteoporotic fracture risk, particularly for hip fracture.

A fundamental relationship exists linking the velocity (v) of a sound wave to the elasticity (E) and density (ρ) of a material, namely, $v=\sqrt{(E/\rho)}$, although the elasticity modulus used in the relationship is dependent on the sound propagation mode; for example, bulk modulus $+4/3$ of the rigidity modulus for the longitudinal wave ($\lambda+4/3\mu$), the rigidity modulus for the shear wave and the Young's modulus for the bar wave. Young's modulus is derived from mechanical testing and longitudinal velocity from ultrasound measurements (Njeh *et al.*, 1996). A similar fundamental relationship does not exist for BUA. It has been shown however that BUA follows a parabolic-type dependence on porosity having a minimum values corresponding to both solid bone (0% porosity) and marrow (100% porosity) (Hodgskinson *et al.*, 1996). Hence, similar BUA values may be obtained for a few marrow pores within a largely solid bone (Sasso *et al.*, 2008) and a few bony trabeculae within a largely marrow sample. A parameter that follows a similar pattern is the surface area of the bone-marrow interface; associated with this, a linear relationship between BUA and fractal dimension has been demonstrated (Langton *et al.*, 1998).

Even though 25 years have passed since BUA was first described (Langton *et al.*, 1984), there remains a lack of a fundamental understanding of the dependence of ultrasound propagation, and BUA, in particular, on the material and structural properties of cancellous bone. In order to elucidate these relationships, a number of theoretical approaches have been considered including scattering, simple mixtures, idealized microstructures, and Biot. Scattering is caused by sudden spatial changes in elastic properties, the magnitude being dependent on relative size of inhomogeneities and the ultrasound wavelength. Multiple scattering may also be considered, being a combination of the original and previously scattered waves (Luppé *et al.*, 2003; Haiat *et al.*, 2008a, 2008b). Boutin (2007) has combined rigid-porous theory and scattering to investigate the low frequency scattering of acoustic wave propagation in heterogeneous media made of air and motionless inclusions. The simple mixture theory expresses velocity in terms of bone volume fraction, density, and bulk modulus. The theory of Chernov (1960) combines scattering and simple mixture theory via velocity fluctuations and scatterer size. Simple mixture theories have had limited success for porous media such as cancellous bone. Two theories that are inherently applicable to a solid framework perfused with a viscous fluid are the Schoenberg and Biot theories. The theory of Schoenberg (1983, 1984, 1986) considers periodically alternating parallel solid-fluid layers, but does not consider the viscous absorption. Biot theory predicts two compressional waves, often referred to as "fast and "slow," when the waves propagating through the solid frame of bone and marrow are in- and out-of-phase, respectively. Biot theory was specifically developed to describe acoustic wave propagation in fluid-saturated porous elastic media (Biot, 1956a, 1956b). Although its original context was geophysical testing of porous rocks, it has been used extensively to describe the wave motion in cancellous bone. It allows for an arbitrary microstructure, with separate motions considered for the solid elastic framework (bone) and the interspersed fluid (marrow), induced by the ultrasonic wave, and also includes energy loss due to viscous friction between solid (bone) and fluid (marrow). In addition to the two compressional waves predicted by Schoenberg's theory, Biot theory also predicts a shear wave. McKelvie and Palmer (1991) were first to apply Biot theory to ultrasonic wave propagation in cancellous bone. Hosokawa and Otani (1997) first observed experimentally the two theoretically predicted compressional waves in cancellous bone at ultrasonic frequencies. Subsequently Biot theory has been used extensively to describe the wave motion in trabecular (cancellous) bone (Haire and Langton, 1999; Fellah *et al.*, 2004; Sebaa *et al.*, 2006). A modified Biot–Attenborough (MBA) model has also been proposed for acoustic wave propagation in a non-rigid porous medium with circular cylindrical pores starting from a formulation for a rigid-framed porous material (Roh *et al.*, 2003; Attenborough 1982, 1983). The MBA has been used to predict the dependences of velocity and attenuation on frequency and porosity in bovine cancellous bone (Lee *et al.* 2003; Lee and Yoon 2006).

For geophysical applications (Carcione 1996), Biot theory has been further developed including semi-analytical approach that allows for transverse anisotropy in the frame elastic moduli, tortuosity and permeability. The angular dependences of phase velocities for the fast and the slow waves in cancellous bone have been predicted (Hughes *et al.* 1999), along with the anisotropic behavior of acoustic wave propagation (Hughes *et al.* 2007). Also the Biot model has been modified to include the acoustic anisotropy of cancellous bone by introducing empirical angle-dependent parameters, and used to predict both the fast and slow wave velocities as a function of propagation angle with respect to the trabecular alignment of cancellous bone (Lee *et al.* 2007).

Most recently, Aygün *et al.* (2009) have extended previous work on the influence of anisotropic pore structure and elasticity in cancellous bone by developing an anisotropic Biot–Allard model, allowing for angle-dependent elasticity and angle-and-porosity dependent tortuosity. The extreme angle dependence of tortuosity corresponding to the parallel plate microstructure used by Hughes *et al.* (2007) has been replaced by angle-and-porosity dependent tortuosity values based on data for slow wave transmission through air-filled stereo-lithography (STL) bone replicas (Attenborough *et al.* 2005). It has been suggested that the anisotropic Biot–Allard model could be used to give further insight into the factors that have the most important influence on the angle dependency of wave speeds and attenuation in cancellous bone.

This paper reports measurements of ultrasonic transmission made through water-saturated bone replicas at 100 kHz and 1 MHz. The resulting data are compared with predictions of a modified Biot–Allard model with anisotropic angle-and-porosity dependent tortuosity and angle-dependent elasticity. First we summarize the theory. Second we present the development of STL bone replicas. Then we present the measurements and default parameters used for the predictions and, finally, we compare data and predictions.

II. THEORY

A porous sample of length L is subjected to an ultrasonic wave in fluid (water) P^i. Part of ultrasonic wave is reflected back into the fluid P^r, while other part is transmitted through the sample P^t. Fellah *et al.* (2004) presented an analytical model based on the Biot's theory modified by Johnson *et al.* (1987) model to describe the viscous interaction between fluid and a porous elastic structure. The Fourier transform of the transmitted field is given by Fellah *et al.* (2004) as

$$P_3(x,\omega) = T(\omega)\exp\left(-j\omega\frac{(x-L)}{c_0}\right)\varphi(\omega), \quad x \geq L, \tag{1}$$

where $\varphi(\omega)$ is the Fourier transform of the incident field $(P^i(t))$, $T(\omega)$ is the Fourier transform of the transmission kernel, ω is the angular frequency of motion, c_0 is the speed of sound in fluid, and L is the thickness of the material. A more detailed consideration of the transformed field can be found in the paper of Fellah *et al.* (2004). The transmission coefficient $T(\omega)$ is given by

$$T(\omega) = \frac{j\omega 2\rho_f c_0 F_4(\omega)}{[j\omega\rho_f c_0 F_4(\omega)]^2 - [j\omega F_3(\omega) - 1]^2}, \tag{2}$$

where $F_4(\omega)$ and $F_3(\omega)$ are given in the Appendix.

The parallel orientation of the trabeculae in cancellous bone means that cancellous bone has transverse anisotropy. Such inherent anisotropy means that the acoustical properties vary with transmission direction (Attenborough *et al.*, 2005). Aygün *et al.* (2009) introduced such anisotropy into Biot–Allard model by allowing angle-and-porosity dependent tortuosity and angle-dependent elasticity. A heuristic form for porosity- and angle-dependent tortuosity is proposed by Aygün *et al.* (2009) as

$$\alpha_\infty = 1 - r\left(1 - \frac{1}{\phi}\right) + k\cos^2(\theta), \tag{3}$$

where ϕ is the porosity, θ is the variable between 0° and 90°, and r and k can be considered adjustable. A range of possible values of r and k have been found by comparing predictions of Eq. (3) for θ=0° and 90°, respectively with values deduced from air-filled replica bones (Attenborough *et al.*, 2005) of known porosity. Values of r and k are found by solving the resulting simultaneous equations.

To predict transmission through an anisotropic poroelastic sample it is necessary to allow for elastic anisotropy also. Williams (1992) suggested that the dependence of skeletal frame modulus (Young's modulus E_b, bulk Modulus K_b, and rigidity modulus μ_b) in terms of bone volume fraction $(1-\phi)$ and the Young's modulus of the solid material of the frame (E_s) are given by $E_b=E_s(1-\phi)^n$, $K_b=E_b/(1-2\upsilon_b)$, and $\mu_b=E_b/(1+2\upsilon_b)$, respectively, where υ_b is the Poisson's ratio of frame and the exponent n varies from 1 to 3 according to Gibson (1985), depending on the angle (θ) with respect to the dominant structural orientation according to $n=n_1\sin^2(\theta)+n_2\cos^2(\theta)$. Values of n_1=1.23 and n_2=2.35 are chosen by Lee *et al.* (2007) to be consistent with the work of Williams (1992). The Biot–Allard model for waves in fluid-saturated poro-elastic media (Allard, 1993) allows for thermal exchange and viscous drag between pore-fluid and the solid framework. Thermal exchange effects between solid and fluid can be included through a frequency-dependent bulk modulus of the fluid. However, whereas thermal effects are fairly important in air-filled porous materials, they are expected to be of minor importance in the water-filled bone replicas.

III. DEVELOPMENT OF STL BONE REPLICAS

Several authors such as Strelitzki *et al.* (1997), Wear (2005), and Lee and Choi (2007) investigated the phase velocities and attenuation in cancellous-bone-mimicking phantoms. Stereo-lithographical bone replicas made of resin have been developed (Langton *et al.*, 1997). STL is a form of rapid prototyping that allows complex solid objects to be manufactured directly from three dimensional (3D) computer models in the form of successive layers of light-cured resin. There are two stages to stereo-lithography: design and manufacturing. During the design stage the required object is initially created using standard 3D solid modeling techniques and then converted into the stereo-lithography format consisting of a series of thin slices. The stereo-lithography manufacturing system consists of a vat of light-sensitive resin with an elevator and computer-controlled scanning laser. At the start of the process, the elevator is positioned just below the surface (typically 0.1 mm) of the liquid stereo-lithography resin. The laser scanner "prints" the bottom layer onto the resin surface, which solidifies upon exposure to the laser beam. The elevator then moves down by an incremental distance, and the stereo-lithography resin is respread over the surface of the vat prior to the next scan. As successive solid layers are formed, they bond to produce a single solid object. When the model is completed the elevator is raised, and the unused resin is allowed to drain. The laser cures the stereo-

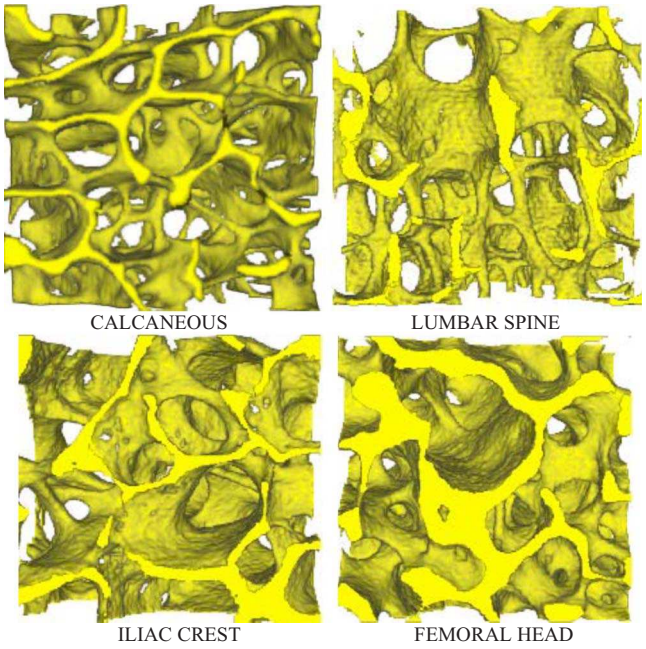

FIG. 1. (Color online) Views of four stereo-lithographical bone replicas.

lithography resin to approximately 60%. The curing process is completed in an ultraviolet oven. The resolution of the stereo-lithography process is governed by the laser spot size and the vertical movement of the elevator. Typically, the laser spot diameter will be better than 0.3 mm, and the elevator movement resolution will be about 2.5 μm. Further details of stereo-lithography technique can be found elsewhere (Langton *et al.* 1997). The views of four stereo-lithographical bone replicas are shown in Fig. 1.

The primary reason for creating stereo-lithography replicas is that multiple copies may be created. This is particularly valuable for mechanical testing, where measurement in one direction may damage a sample and preclude testing in other orthogonal directions. The models were created at a magnification of $\times 13$ to ensure spatial fidelity between the voxel size of the microCT scan of the original natural tissue samples and the minimum wall thickness achievable with STL. Bone "corrosion" due to osteoporosis can be simulated physically by corresponding stereo-lithographical bone replicas. Therefore bone replicas should enable studies of the acoustical effects of changes in microstructure. Since the

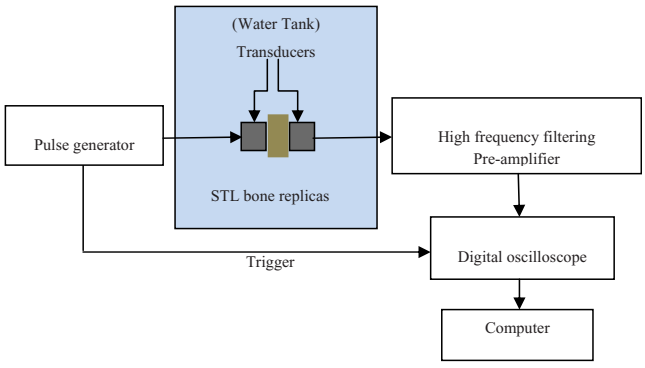

FIG. 2. (Color online) Experimental setup for ultrasonic measurements (Fellah *et al.*, 2004).

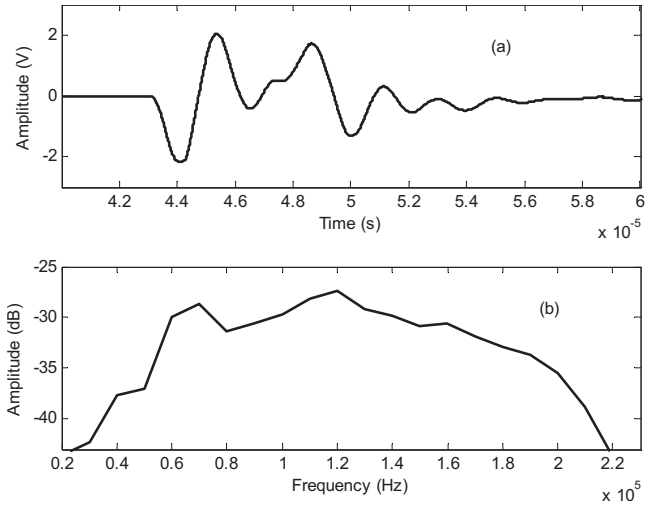

FIG. 3. (a) Incident (reference) signal versus time; (b) spectrum of the Incident signal versus frequency, 100 kHz transducer.

STL bone replicas used in measurements have 13 times the actual size of the bone microstructure, spatial matching between sample microstructure and ultrasound wavelengths could be achieved by lowering the frequency. Hence 1 MHz should be reduced to approximately 100 kHz. To simulate the 200–600 kHz measurements used in BUA, it would be necessary to use between 15.4 and 46.2 kHz.

IV. MEASUREMENTS

The experimental procedure used by Fellah *et al.* (2004) has been followed to perform measurements in a water tank (see Fig. 2). Two broadband Panametrics A 303S plane piezoelectric transducers having 1 cm diameter with 1 MHz central frequency, and two Panametrics V3052 transducers having 44 mm diameter with 100 kHz central frequency have been used for experiments. 400 V pulses are provided by a 5058PR Panametrics pulser/receiver. Electronic interference is removed by 1000 acquisition averages.

When a wave impinges on a STL bone replica, part of the wave is reflected back. The part of the wave penetrating

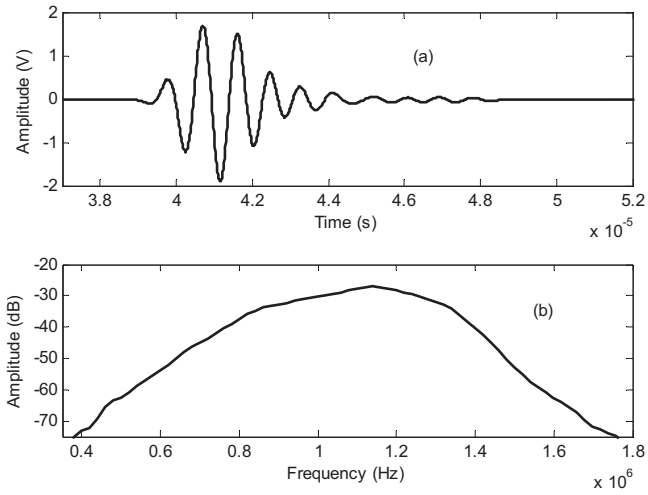

FIG. 4. (a) Incident (reference) signal versus time; (b) spectrum of the Incident signal versus frequency, 1MHz transducer.

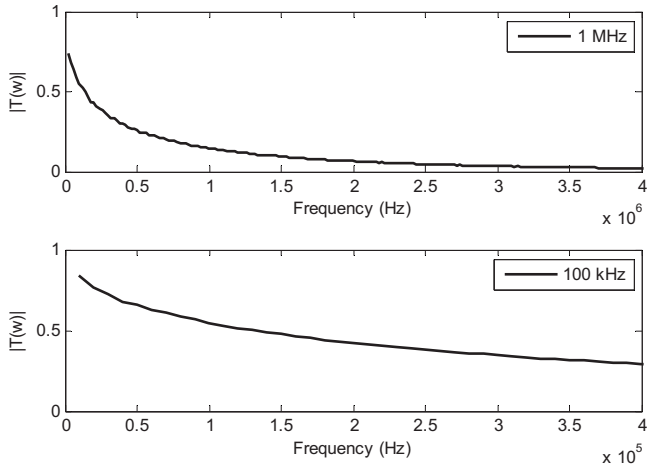

FIG. 5. Numerical simulation of the transmission coefficient versus frequency at 100 kHz and 1 MHz.

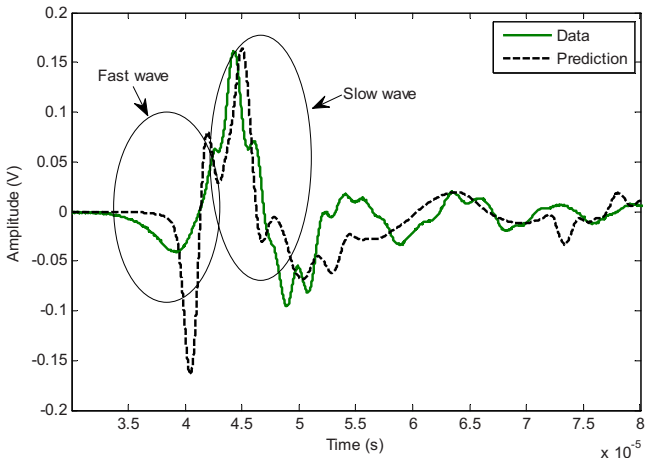

FIG. 6. (Color online) Comparison of predicted and measured transmitted waveforms through a water-saturated ICF bone replica at 100 kHz.

into the sample undergoes mode conversion into fast and slow components, which are transmitted through the STL bone replica. The measurements have been made parallel to the trabeculae direction. The stereo-lithographical bone replicas used in the measurements are in the form of 57 mm cubes. The incident (reference) signals generated by 100 kHz and 1 MHz transducers and transmitted through fluid (water) are shown in Figs. 3(a) and 4(a), and their spectra are shown in Figs. 3(b) and 4(b), respectively. Predicted transmission coefficients in frequency domain for lumbar spine (LS2B) at 100 kHz and 1 MHz are shown in Fig. 5.

V. COMPARISONS BETWEEN DATA AND PREDICTIONS

The parameters used in the predictions are listed in Table I. The elastic moduli of the STL bone replicas made of resin have been taken to be equal to the elastic modulus of resin which is 6.04 GPa (DSM Somos) and is smaller than the elastic modulus of real bone, which is 20 GPa (Williams 1992). Assuming that the permeability of the bone is 5×10^{-9} m^3 (McKelvie and Palmer 1991), the permeability of bone replicas has been taken to be 13^2 times higher because of the magnification of the actual size of the bone microstructure by 13 times in each direction. The assumed characteristics of the saturating fluid (water) are: density $\rho_f = 1000$ kg/m^{-3}, viscosity $\eta = 10^{-3}$ kg ms^{-1}, and speed of sound in water $c_0 = 1490$ m/s.

Measured and predicted transmitted signals are traveling through the bone replicas in the same direction as the trabecular alignment (x direction). The incident signal shown in Fig. 3 has been used for predictions. Predicted transmitted waves of STL iliac crest (ICF), femoral head (FRA), and LS2B replicas versus time are compared with measured transmitted waves in water at 100 kHz in Figs. 6–8, respectively. In Fig. 6 the initial parts of the measured and predicted transmitted waveforms can be identified as the fast wave arrival, while the second and major parts of the transmitted waveforms can be identified as the slow wave contribution. Although two compressional wave arrivals can be observed in both data and predictions in Fig. 6, they can be observed only in the predictions in Fig. 7, and in the data in Fig. 8. While the agreement between the overall structure of the waveform data and predictions is reasonable, the magnitude of the leading negative spike is consistently overestimated by the predictions, and the trailing parts of the pulses are not predicted very accurately. The root mean square errors between predictions and data have been calculated. The error for FRA, ICF, and LS2B bone replicas are 0.021, 0.01, and 0.016 V at 100 kHz, respectively.

Predicted transmitted waveforms through water-filled STL FRA, ICF, LS2B, and CAB replicas are compared with measured transmitted waves in water at 1 MHz in Figs. 9–12, respectively. Although the predicted and measured transmitted waveforms are similar, there are significant differences between the predicted and measured transmitted

TABLE I. Default input parameters for STL bone replicas.

Parameters	Iliac crest ICF	Femoral head FRA	Lumbar spine LS2	Calcaneus CAB
Density of replica ρ_s (Attenborough *et al.*, 2005)	1233.4 kg/m^3	1227 kg/m^3	1206.6 kg/m^3	1171 kg/m^3
Young's modulus E_s (DSM Somos)	6.04 GPa	6.04 GPa	6.04 GPa	6.04 GPa
Poisson's ratio of solid υ_s	0.30	0.30	0.30	0.30
Poisson's ratio of frame υ_b	0.36	0.40	0.38	0.34
Porosity ϕ (Attenborough *et al.*, 2005)	0.8386	0.7426	0.9173	0.8822
Permeability k_0	845×10^{-9} m^3	845×10^{-9} m^3	845×10^{-9} m^3	845×10^{-9} m^3
Viscous characteristic length Λ	100 μm	60 μm	220 μm	150 μm
r (Aygün *et al.*, 2009)	0.888	0.591	0.521	0.816
k (Eq. (3))	0.468	0.684	0.143	0.574

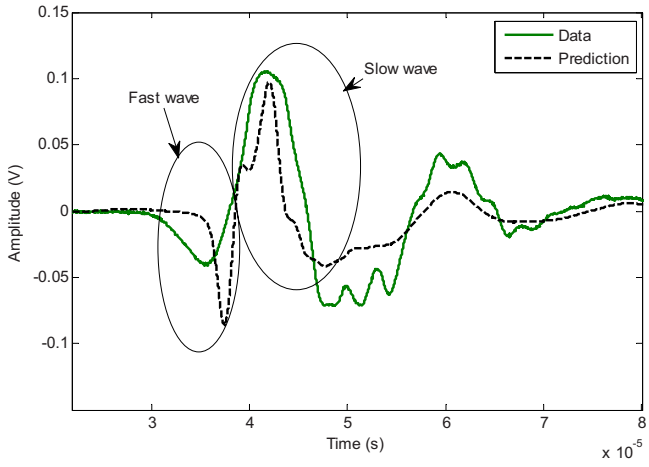

FIG. 7. (Color online) Comparison of predicted and measured transmitted waveforms through a water-saturated FRA bone replica at 100 kHz.

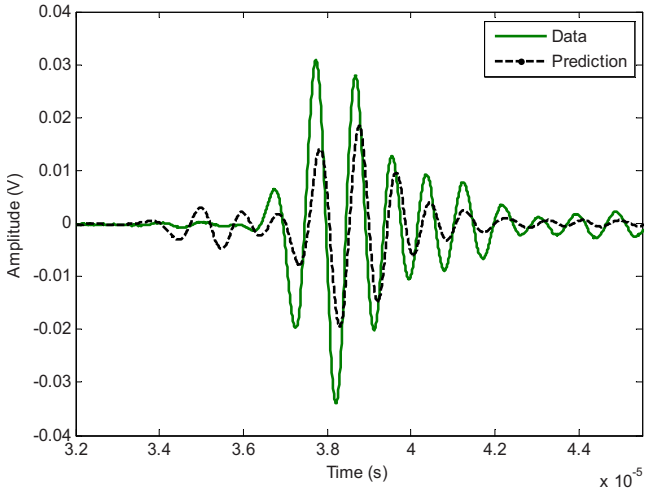

FIG. 9. (Color online) Comparison of predicted and measured transmitted waveforms through a water-saturated FRA bone replica at 1 MHz.

amplitudes at 1 MHz. The root mean square error between predictions and data for CAB, FRA, ICF, and LS2B bone replicas are 0.00188, 0.0031, 0.0049, and 0.0055 V at 1 MHz, respectively. The measured amplitudes of transmitted waveforms through the femoral head and iliac crest replicas are larger than the predicted ones, while those measured through the lumbar spine and calcaneus replicas are smaller than the predicted ones. In the latter two cases, the fact that the measured amplitudes are smaller than predicted could be attributed to the effects of scattering, which should give rise to additional attenuation. This interpretation is not consistent with the cases where the measured transmitted amplitudes are larger than the predicted ones. The lack of consistency in the agreement between predictions and data might be related to the assumption that the permeabilities of the replicas are all the same, whereas the known differences in porosity should be reflected in differences in permeability. Moreover, scattering can be expected to be more important when the typical dimensions of the frame and pore microstructure are larger. In this respect it is interesting to note that the lumbar spine and calcaneus bone replicas have higher fitted viscous characteristic lengths than the femoral head and iliac crest bone replicas. Porosity and density of STL bone replicas are given by Attenborough *et al.* (2005). The values of r for all STL bone replicas are given by Aygün *et al.* (2009). Only two parameters, Poisson's ratio of frame and viscous characteristic length, were adjusted in order to obtain the "best-fit." In particular, the predictions are very sensitive to the assumed values of viscous characteristic length. The "best-fit" characteristic length values (Table I) for the replicas are about 13 times those found for real bone in the literature i.e., between 5 and 10 μm (Fellah *et al.*, 2004; Sebaa *et al.*, 2006).

VI. DISCUSSION AND CONCLUSION

The use of stereo-lithograpical bone replicas made from resin has the potential to enable systematic investigations of the influences of perforation and thinning in cancellous bone on the acoustical and mechanical properties of the bone structure. Waves transmitted through STL bone replicas with higher porosity values have higher amplitudes. Osteoporotic

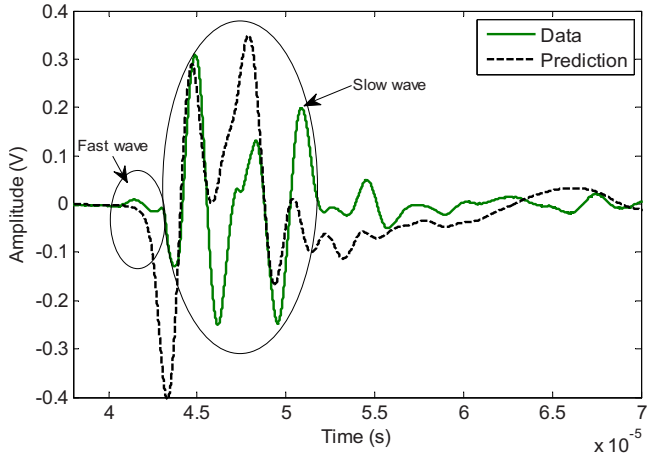

FIG. 8. (Color online) Comparison of predicted and measured transmitted waveforms through a water-saturated LS2B bone replica at 100 kHz.

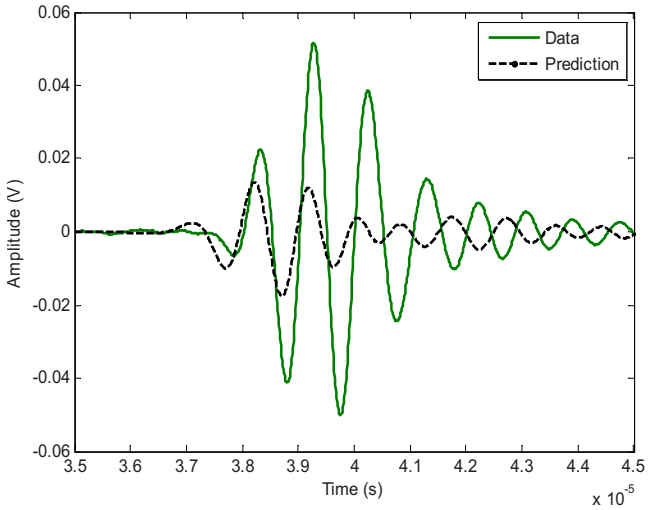

FIG. 10. (Color online) Comparison of predicted and measured transmitted waveforms through a water-saturated ICF bone replica at 1 MHz.

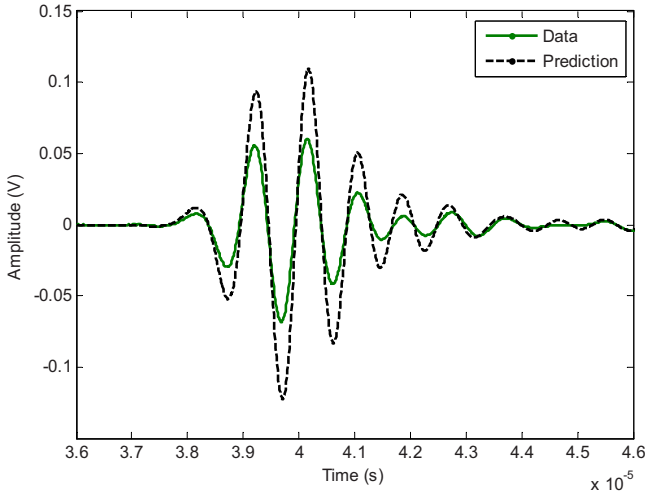

FIG. 11. (Color online) Comparison of predicted and measured transmitted waveforms through a water-saturated LS2B bone replica at 1 MHz.

bones will have higher porosity values due to bone loss, so greater energy will be transmitted through them in comparison with normal bone.

A consequence of using replica bones, which are 13 times the actual size of the bone microstructure, is that scattering should become important at lower frequencies than in measurements with real bone samples. Transmitted signals for water-saturated stereo-lithograpical bone replicas have been predicted by modified anisotropic Biot–Allard model, which neglects scattering, and the results have been compared to measurements made in a water-filled tank at 100 kHz and 1 MHz. The wavelengths of the slow and fast waves in water-saturated STL bone replicas at 100 kHz are 15 and 30 mm, respectively. These wavelengths are comparable with the dimensions of microstructural elements of STL bone replicas. According to Williams (1992), the pore sizes in cancellous bone vary between 0.5 and 1 mm, so typical trabeculae widths in the replicas vary between 6.5 and 13 mm. Remarkably, scattering seems not to cause significant discrepancies between predictions and data at 100 kHz (which would be equivalent to 1.3 MHz in real bone), perhaps as a consequence of the fact that the samples behave as low pass filters. Scattering should be even more important at 1 MHz (equivalent to 13 MHz in real bone), where the fast and slow wavelengths are 3 and 1.5 mm, respectively. So the agreement between predictions and data is rather surprising.

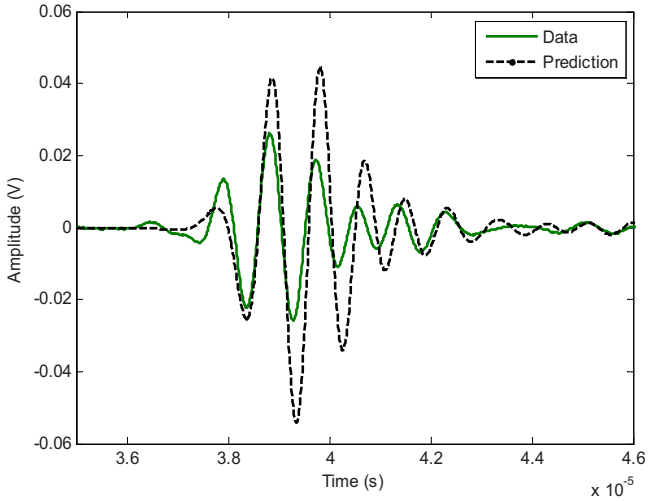

FIG. 12. (Color online) Comparison of predicted and measured transmitted waveforms through a water-saturated CAB bone replica at 1 MHz.

These data and predictions support further use of Biot-based theories and of STL replicas for studying ultrasonic transmission through bone.

ACKNOWLEDGMENT

This paper has been supported by Leverhulme Grant No. F/00 181/N, which provided for collaboration with the Laboratory of Acoustics and Thermal Physics at Leuven where the data reported here were obtained.

APPENDIX: BASIS FOR THE PREDICTION OF THE TRANSMISSION COEFFICIENT

The transmission coefficient $T(\omega)$ is given by Fellah *et al.* (2004)

$$T(\omega) = \frac{j\omega 2\rho_f c_0 F_4(\omega)}{[j\omega\rho_f c_0 F_4(\omega)]^2 - [j\omega F_3(\omega) - 1]^2},$$

where

$$F_i(\omega) = \{1 + \phi[\Im_i(\omega) - 1]\} x\sqrt{\lambda_i(\omega)} \times \frac{\Psi_i(\omega)}{\sinh(l\sqrt{\lambda_i(\omega)})} \frac{2}{\Psi(\omega)}, \quad i = 1,2,$$

$$F_3(\omega) = \rho_f c_0 \{F_1(\omega)\cosh[l\sqrt{\lambda_1(\omega)}] + F_2(\omega)\cosh[l\sqrt{\lambda_2(\omega)}]\},$$

$$F_4(\omega) = F_1(\omega) + F_2(\omega),$$

The eigenvalues $\lambda_1(\omega)$ and $\lambda_2(\omega)$ are the squared complex wave numbers of the two compressional waves and are given by

$$\lambda_1(\omega) = \frac{1}{2}[-\tau_1\omega^2 + \tau_2(j\omega)^{3/2} - \sqrt{(\tau_1^2 - 4\tau_3)\omega^4 + 2(\tau_1\tau_2 - 2\tau_4)(j\omega)^{7/2} + \tau_2^2(j\omega)^3}],$$

$$\lambda_2(\omega) = \frac{1}{2}[-\tau_1\omega^2 + \tau_2(j\omega)^{3/2} + \sqrt{(\tau_1^2 - 4\tau_3)\omega^4 + 2(\tau_1\tau_2 - 2\tau_4)(j\omega)^{7/2} + \tau_2^2(j\omega)^3}],$$

where

$$\tau_1 = R'\rho_{11} + P'\rho_{22} - 2Q'\rho_{12},$$

$$\tau_2 = 2(R' + P' + 2Q'),$$

$$\tau_3 = (R'P' - Q'^2)(\rho_{11}\rho_{22} - \rho_{12}^2),$$

and

$$\tau_4 = A(R'P' - Q'^2)(\rho_{11} + \rho_{22} - 2\rho_{12}).$$

Coefficients R', P', and Q' are given by

$$R' = \frac{R}{PR - Q^2},$$

$$Q' = \frac{Q}{PR - Q^2},$$

and

$$P' = \frac{P}{PR - Q^2},$$

where P, R, and Q are generalized elastic constants.

The eigenvectors $\mathfrak{I}_1(\omega)$ and $\mathfrak{I}_2(\omega)$ are given by

$$\mathfrak{I}_1(\omega) = \frac{(2\tau_5 - \tau_1)\omega^2 + (\tau_2 - 2\tau_6)(j\omega)^{3/2} - \sqrt{(\tau_1^2 - 4\tau_3)\omega^4 + 2(\tau_1\tau_2 - 2\tau_4)(j\omega)^{7/2} + \tau_2^2(j\omega)^3}}{2[-\tau_7\omega^2 - \tau_6(j\omega)^{3/2}]},$$

$$\mathfrak{I}_2(\omega) = \frac{(2\tau_5 - \tau_1)\omega^2 + (\tau_2 - 2\tau_6)(j\omega)^{3/2} + \sqrt{(\tau_1^2 - 4\tau_3)\omega^4 + 2(\tau_1\tau_2 - 2\tau_4)(j\omega)^{7/2} + \tau_2^2(j\omega)^3}}{2[-\tau_7\omega^2 - \tau_6(j\omega)^{3/2}]},$$

where

$$\tau_5 = (R'\rho_{11} - Q'\rho_{12}),$$

$$\tau_6 = A(R' + Q'),$$

$$\tau_7 = (R'\rho_{12} - Q'\rho_{22}).$$

The coefficients $\Psi_1(\omega)$, $\Psi_2(\omega)$, and $\Psi(\omega)$ are given by

$$\Psi_1(\omega) = \phi Z_2(\omega) - (1 - \phi)Z_4(\omega),$$

$$\Psi_2(\omega) = (1 - \phi)Z_3(\omega) - \phi Z_1(\omega),$$

$$\Psi(\omega) = 2[Z_1(\omega)Z_4(\omega) - Z_2(\omega)Z_3\omega)],$$

and the coefficients $Z_1(\omega)$, $Z_2(\omega)$, $Z_3(\omega)$, and $Z_4(\omega)$ by

$$Z_1(\omega) = [P + Q\mathfrak{I}_1(\omega)]\lambda_1(\omega),$$

$$Z_2(\omega) = [P + Q\mathfrak{I}_2(\omega)]\lambda_2(\omega),$$

$$Z_3(\omega) = [Q + R\mathfrak{I}_1(\omega)]\lambda_1(\omega),$$

$$Z_4(\omega) = [Q + R\mathfrak{I}_2(\omega)]\lambda_2(\omega).$$

Allard, J. F. (**1993**). *Propagation of Sound in Porous Media: Modelling Sound Absorbing Materials* (Chapman and Hall, London).

Attenborough, K. (**1982**). "Acoustical characteristics of porous materials," Phys. Rep. **82**, 179–227.

Attenborough, K. (**1983**). "Acoustic characteristics of rigid fibrous absorbents and granular materials," J. Acoust. Soc. Am. **73**, 785–799.

Attenborough, K., Qin, Q., Fagan, M. J., Shin, H.-C., and Langton, C. M. (**2005**). "Measurements of tortuosity in stereolithographical bone replicas using audio-frequency pulses," J. Acoust. Soc. Am. **118**, 2779–2782.

Aygün, H., Attenborough, K., Postema, M., Lauriks, W., and Langton, C. M. (**2009**). "Predictions of angle dependent tortuosity and elasticity effects on sound propagation in cancellous bone," J. Acoust. Soc. Am. **126**, 3286–3290.

Biot, M. A. (**1956a**). "Theory of propagation of elastic waves in a fluid saturated porous solid, I. Low frequency range," J. Acoust. Soc. Am. **28**, 168–178.

Biot, M. A. (**1956b**). "Theory of propagation of elastic waves in a fluid saturated porous solid, II. High frequency range," J. Acoust. Soc. Am. **28**, 179–191.

Boutin, C. (**2007**). "Rayleigh scattering of acoustic waves in rigid porous media," J. Acoust. Soc. Am. **122**, 1888–1905.

Carcione, J. (**1996**). "Wave propagation in anisotropic, saturated porous media: Plane-wave theory and numerical simulation," J. Acoust. Soc. Am. **99**, 2655–2666.

Chernov, L. A. (**1960**). *Wave Propagation in a Random Medium* (McGraw-Hill, New York).

DSM Somos, The ProtoFunctional Materials Company, WaterClear 10110.

Fellah, Z. E. A., Chapelon, J. Y., Berger, S., Lauriks, W., and Depollier, C. (**2004**). "Ultrasonic wave propagation in human cancellous bone: Application of Biot theory," J. Acoust. Soc. Am. **116**, 61–73.

Frost, M. L., Blake, G. M., and Fogelman, I. (**2001**). "Quantitative ultrasound and bone mineral density are equally strongly associated with risk factors for osteoporosis," J. Bone Miner. Res. **16**, 406–416.

Gibson, L. J. (**1985**). "The mechanical behaviour of cancellous bone," J. Biomech. **18**, 317–328.

Haiat, G., Lhémery, A., and Renaud, F. (**2008a**). "Velocity dispersion in trabecular bone: Influence of multiple scattering and of absorption," J. Acoust. Soc. Am. **124**, 4047–4058.

Haiat, G., Lhémery, A., Padilla, F., Laugier, P., and Naili, S. (**2008b**). "Modeling of "anomalous" velocity dispersion in trabecular bone: Effect of multiple scattering and of viscous absorption," in Proceedings of the Euro-Noise, Paris.

Haiat, G., Padilla, F., Cleveland, R. O., and Laugier, P. (**2006**). "Effects of frequency-dependent attenuation and velocity dispersion on in vitro ultrasound velocity measurements in intact human femur specimens," IEEE Trans. Ultrason. Ferroelectr. Freq. Control **53**, 39–51.

Haire, T. J., and Langton, C. M. (**1999**). "Biot theory: A review of its application on ultrasound propagation through cancellous bone," Bone **24**, 291–295.

Hodgskinson, R., Njeh, C. F., Whitehead, M. A., and Langton, C. M. (**1996**). "Non-linear relationship between BUA and porosity in cancellous bone mimics," Phys. Med. Biol. **41**, 2411–2420.

Hosokawa, A., and Otani, T. (**1997**). "Ultrasonic wave propagation in bovine cancellous bone," J. Acoust. Soc. Am. **101**, 558–562.

Hughes, E. R., Leighton, T. G., Petley, G. W., and White, P. R. (**1999**). "Ultrasonic propagation in cancellous bone: A new stratified model," Ultrasound Med. Biol. **25**, 811–821.

Hughes, E. R., Leighton, T. G., White, P. R., and Petley, G. W. (**2007**). "Investigation of an anisotropic tortuosity in a Biot model of ultrasonic propagation in cancellous bone," J. Acoust. Soc. Am. **121**, 568–574.

Johnson, D. L., Koplik, J., and Dashen, R. (**1987**). "Theory of dynamic permeability and tortuosity in fluid-saturated porous media," J. Fluid Mech. **176**, 379–402.

Lang, T. (**2004**). "Quantitative computed tomography," in *The Physical Measurement of Bone*, edited by C. M. Langton and C. F. Njeh (IOPP, Bristol, UK), pp. 308–318.

Langton, C. M., Palmer, S. B., and Porter, R. W. (**1984**). "The measurement

of broadband ultrasonic attenuation in cancellous bone," Eng. Med. **13**, 89–91.
Langton, C. M., Whitehead, M. A., Haire, T. J., and Hodgskinson, R. (**1998**). "Fractal dimension predicts broadband ultrasound attenuation in stereolithography models of cancellous bone," Phys. Med. Biol. **43**, 467–471.
Langton, C. M., Whitehead, M. A., Langton, D. K., and Langley, G. (**1997**). "Development of a cancellous bone structural model by stereolithography for ultrasound characterisation of the calcaneus," Med. Eng. Phys. **19**, 599–604.
Lee, K. I., and Choi, M. J. (**2007**). "Phase velocity and normalized broadband ultrasonic attenuation in polyacetal cuboid bone-mimicking phantoms," J. Acoust. Soc. Am. **121**, EL263–EL269.
Lee, K. I., Hughes, E. R., Humphery, V. F., Leighton, T. G., and Choi, M. J. (**2007**). "Empirical angle-dependent Biot and MBA models for acoustic anisotropy in cancellous bone," Phys. Med. Biol. **52**, 59–73.
Lee, K. I., Roh, H.-S., and Yoon, S. W. (**2003**). "Acoustic wave propagation in bovine cancellous bone: Application of the Modified Biot–Attenborough model," J. Acoust. Soc. Am. **114**, 2284–2293.
Lee, K. I., and Yoon, S. W. (**2006**). "Comparison of acoustic characteristics predicted by Biot's theory and the modified Biot–Attenborough model in cancellous bone," J. Biomech. **39**, 364–368.
Luppé, F., Conoir, J. M., and Franklin, H. (**2003**). "Multiple scattering in a trabecular bone: Influence of the marrow viscosity on the effective properties," J. Acoust. Soc. Am. **113**, 2889–2892.
McKelvie, M. L., and Palmer, S. B. (**1991**). "The interaction of ultrasound with cancellous bone," Phys. Med. Biol. **36**, 1331–1340.
Njeh, C. F., Boivin, C. M., and Langton, C. M. (**1997**). "The role of ultrasound in the management of osteoporosis: a review," Osteoporos. Int. **7**, 7–22.
Njeh, C. F., Hodgskinson, R., Currey, J. D., and Langton, C. M. (**1996**). "Orthogonal relationships between ultrasonic velocity and material properties of bovine cancellous bone," Med. Eng. Phys. **18**, 373–381.
Njeh, C. F., and Shepherd, J. A. (**2004**). "Absorptiometric measurement," in *The Physical Measurement of Bone*, edited by C. M. Langton and C. F. Njeh, (IOPP, Bristol, UK), pp. 267–307.
Pothuaud, L., and Majumdar, S. (**2004**). "Magnetic resonance imaging," in *The Physical Measurement of Bone*, edited by C. M. Langton and C. F. Njeh, (IOPP, Bristol, UK), pp. 379–411.
Roh, H. S., Lee, K. I., and Yoon, S. W. (**2003**). "Acoustic characteristics of a non-rigid porous medium with circular cylindrical pores," J. Korean Phys. Soc. **45**, 55–62.
Rosen, C. J. (**2004**). "Anatomy, physiology and disease," in *The Physical Measurement of Bone*, edited by C. M. Langton and C. F. Njeh, (IOPP, Bristol, UK), pp. 3–34.
Sasso, M., Haiat, G., Yamato, Y., Naili, S., and Matsukawa, M. (**2008**). "Dependence of ultrasonic attenuation on bone mass and microstructure in bovine cortical bone," J. Biomech. **41**, 347–355.
Schoenberg, M. (**1983**). "Wave propagation in a finely laminated periodic elastoacoustic medium," Appl. Phys. Lett. **42**, 350–352.
Schoenberg, M. (**1984**). "Wave propagation in alternating solid and fluid layers," Wave Motion **6**, 303–320.
Schoenberg, M. (**1986**). "Wave propagation in alternating solid and viscous fluid layers: Size effects in attenuation and dispersion of fast and slow waves," Appl. Phys. Lett. **48**, 1249–1251.
Sebaa, N., Fellah, Z., Fellah, M., Ogam, E., Wirgin, A., Mitri, F., Depollier, C., and Lauriks, W. (**2006**). "Ultrasonic characterisation of human cancellous bone using the Biot theory: Inverse problem," J. Acoust. Soc. Am. **120**, 1816–1824.
Strelitzki, R., Evans, J. A., and Clarke, A. J. (**1997**). "The influence of porosity and pore size on the ultrasonic properties of bone investigated using a phantom material," Osteoporosis Int. **7**, 370–375.
Thomsen, J. S., Ebbesen, E. N., and Mosekilde, L. (**2002**). "Age-related differences between thinning of horizontal and vertical trabeculae in human lumbar bone as assessed by a new computerized method," Bone **31**, 136–142.
Wear, K. A. (**2005**). "The dependences of phase velocity and dispersion on the trabecular thickness and spacing in trabecular bone-mimicking phantoms," J. Acoust. Soc. Am. **118**, 1186–1192.
Williams, J. L. (**1992**). "Ultrasonic wave propagation in cancellous and cortical bone: Predictions of some experimental results by Biot's Theory," J. Acoust. Soc. Am. **91**, 1106–1112.